Trans-regime Structural Transition of (In^{3+}+Nb^{5+}) Co-doped Anatase TiO$_2$ Nanocrystals under High Pressure

Qingbo Sun[1], Larissa Q. Huston[2], Terry J. Frankcombe[3], Jodie E. Bradby[2], Teng Lu[1],

Dehong Yu[4], Chao Zhou[5], Zhenxiao Fu[5] and Yun Liu[1,*]

[1] Research School of Chemistry, the Australian National University, ACT, 2601, Australia.

[2] Research School of Physics and Engineering, the Australian National University, ACT, 2601, Australia.

[3] School of Physical, Environmental and Mathematical Sciences, University of New South Wales, ACT, 2601, Australia.

[4] Australian Nuclear Science and Technology Organisation, Lucas Height, NSW, 2234, Australia.

[5] Fenghua Advanced Technology Holding Co., Ltd., China.

ABSTRACT: Chemical co-doping and high pressure reaction have been broadly used to synthesize novel materials or tune the physicochemical properties of traditional materials. Here, we take In^{3+} and Nb^{5+} ions co-doped anatase TiO$_2$ nanocrystals as an example and report that a combination of both chemical and high pressure reaction route is more powerful for the preparation of metastable polymorphs. It is experimentally demonstrated that In^{3+} and Nb^{5+} co-doping significantly changes the high-pressure reaction behaviours of anatase TiO$_2$ nanocrystals (<10 nm) and leads to their trans-regime structural

* Corresponding author: Yun.liu@anu.edu.au.

transition in terms of *in situ* Raman analysis, from anatase to a baddeleyite-like phase under compressive pressures and then to an α-PbO$_2$-like structure under decompressive pressures. This abnormal phase transition is attributed to the defect-induced heterogeneous nucleation mechanism. Furthermore, the stiffness of co-doped TiO$_2$ nanocrystals is significantly enhanced due to the synergistic effects of co-dopants. This research not only proposes a potentially effective strategy to synthesize co-doped metastable polymorphic phases but also suggests one feasible method to improve the mechanical properties of anatase TiO$_2$ nanocrystals.

INTRODUCTION

Many traditional materials display abnormal physical behaviours under or after high pressure (HP) reaction as a consequence of the shrinkage of average interatomic distances and the densification of atomic/ionic packing. For example, pressurized titanium dioxide (TiO$_2$) can achieve ultra-hardness comparable to diamond or cubic BN.[1-3] The band-gap of TiO$_2$ can be narrowed to greatly improve photo-reaction activity after HP treatment.[4,5] The superconductivity of Fe-based superconductors (*e.g.* CaFe$_2$As$_2$ or BaFe$_2$As$_2$) can also be controlled by applied pressure.[6] HP reaction is thus not only a valid way to discover novel properties of normal materials but also a critical approach to synthesize new materials with higher coordination numbers.[7]

TiO$_2$ is a typical multiple polymorphic example and is now extensively used in the fields of photo-catalysts, solar cells, cosmetics and electronic devices. Anatase, rutile and brookite are its three common phases and can be synthesized at ambient conditions. Other polymorphs of TiO$_2$ such as baddeleyite-like structure or α-PbO$_2$-like phase can only be prepared under tens of gigapascals (GPa) pressures.[8] The hexagonal Fe$_2$P-type, fluorite and pyrite structures are either predicted theoretically or only observed under extreme HP conditions.[9] Previous HP investigations suggested that the structural transition of anatase TiO$_2$ was strongly dependent on its initial crystallite sizes and smaller crystals kept anatase stable to higher pressures. Figure 1 shows the size-dependent compression and decompression phase diagrams of anatase TiO$_2$, summarized from the literature.[8-10] Three size regimes (<11 nm, 11-40 nm and >40 nm)

are categorized. (1) For those small nanocrystals with crystallite sizes less than 11 nm, pressurization-induced amorphization occurs at ~24 GPa due to the crystal-liquid transformation. On depressurization, the HP disordered phase changes at ~15 GPa from high-density amorphous state (HDA) to a low-density amorphous structure (LDA). (2) For TiO_2 nanocrystals with crystallite sizes between 11 and 40 nm, a direct phase transformation from anatase to a monoclinic baddeleyite-like structure happens during compression at ~16 GPa. This HP-induced baddeleyite-like structure then changes to an α-PbO_2-like phase at ~10.5 GPa when the pressure is gradually released. (3) For TiO_2 nanocrystals with crystallite sizes over 40 nm, they transform from anatase to an α-PbO_2-like phase at ~4.5 GPa and then to a baddeleyite-like structure at ~13 GPa during compression. Similar to the 11-40 nm nanocrystals, the baddeleyite-like structure also becomes an α-PbO_2-like phase after decompression, but starts at a lower onset pressure of ~7 GPa. After the whole compression and decompression cycle, the anatase structure of TiO_2 can not be recovered. The pressure values, which are applied on micro/nanoparticles with a similar size range for structural transition, remain almost unchanged between two successive phases except for a small fluctuation caused by the pressure calibration method, the transmitting medium or the original properties of anatase TiO_2.

Doping foreign ions/atoms into the crystal structures of host materials inevitably affects their macroscopic properties as it strategically changes the chemical environment of doped sites and thus varies structural stability. Some dopants (*e.g.* Mn in ZnO nanowires[11] or Sc/Y in AlN nanoprisms[12]) drastically reduce the onset formation pressure of related new polymorphs while other dopants such as Mg in lanthanum silicate[13] significantly elevate the critical pressure of phase transition. Our recent study indicated that co-doping In^{3+} and Nb^{5+} ions introduced defect clusters into rutile TiO_2 and thus enabled the localization of electrons in certain regions through creating electron pinned defect dipoles for colossal permittivity.[14] Given the complicated pressure-induced phase transition scenarios of anatase TiO_2, the simultaneous introduction of In^{3+} and Nb^{5+} ions into their crystal structures might also affect high pressure reaction dynamics and possibly generate special polymorphs of co-doped TiO_2. Moreover, the ionic radius of In^{3+}

ions is significantly larger than that of host Ti^{4+} ions. The introduction of large-size dopants would result in the great distortion of the local crystal structure and thus change the stiffness of host TiO_2 materials in a similar way to the well-known Y stabilized ZrO_2. Here, we experimentally design an effective approach to cooperatively introduce In^{3+} and Nb^{5+} ions (~5at.%, compared to titanium ions) into small anatase TiO_2 nanocrystals (<10 nm). High pressure reaction behaviour of co-doped nanocrystals is systematically investigated by an *in situ* Raman spectroscopy. The enhanced stiffness (incompressibility) by co-doping is analysed and the associated mechanism for the abnormal structural transition behaviour is also discussed based on defect-induced heterogeneous nucleation mechanism.

EXPERIMENTAL SECTION

Materials. (In^{3+}+Nb^{5+}) co-doped anatase TiO_2 nanocrystals were synthesized by a solvothermal method and they are directly used for high pressure reaction. Detailed information about the preparation of these co-doped nanocrystals will be described elsewhere.[15]

High Pressure Process. A diamond anvil cell with a cullet size of 400 µm was employed to conduct the high pressure reaction. A steel gasket of 30 µm in thickness was drilled at the centre to form a 200 µm diameter hole. It served as the sample chamber. (In^{3+}+Nb^{5+}) co-doped anatase TiO_2 nanopowders and two small ruby balls were loaded into the above chamber. A mixture of ethanol and methanol (4:1) were used as a pressure transmitting medium. Samples were carefully loaded to the maximum pressure of 47.2 GPa in small steps.

Characterization Methods

X-ray powder diffraction pattern (XRPD) was collected by PANalytical's X-ray diffractometers with CuKα radiation (λ=1.5406 Å). A field-emission transmission electron microscope (TEM, JEOL-2100F) was utilized to analyse their microscopic morphology and crystallite sizes. The chemical valences and doping levels of In^{3+} and Nb^{5+} ions are analysed by X-ray photoelectron spectroscopy (XPS), energy dispersive spectroscopy (EDS) of scanning electron microscope (SEM) as well as inductively coupled

plasma optical emission spectrometer (ICP-OES). The pressure inside the diamond cell was determined by the pressure dependent shift of the ruby fluorescence R_1 line.[16] *In situ* Raman measurement was taken using a Renishaw Raman System (532 nm laser).

RESULTS and DISCUSSION

Figure 2a shows the XRPD pattern of solvothermal products. All diffraction peaks are assigned to the tetragonal phase with space group symmetry $I4_1/amd$. We experimentally demonstrate the nature of pure anatase phase for the synthesized solvothermal products. Their crystallite size is estimated to be about 6.8 nm according to the calculation using the Scherrer equation,[17] and further confirmed by the direct observation from a high resolution TEM image (ranging from 4.7 nm to 10.8 nm and having an average crystallite size of ~6.4 nm, Figure 2b). Moreover, most of the co-doped TiO_2 nanocrystals present a quasi-spherical shape. The respective chemical valences of indium and niobium in the quasi-spherical nanoparticles are +3 and +5, respectively, and that of titanium are composed of +3 and +4, as shown by XPS analysis (Figure 2c and 2d). The total doping concentration of In^{3+} (In/Ti) and Nb^{5+} ions (Nb/Ti) is found to be very close to ~10 at.% and their individual one is ~5 at.% in terms of the results of XPS, EDS of SEM and ICP-OES measurement (Supporting Information, Table S1). It is thus claimed that ($In^{3+}+Nb^{5+}$) co-doped TiO_2 nanocrystals used as HP reactants of this work have the respective doping concentration of 5 at.%, anatase phase, quasi-spherical morphology and the average crystallite sizes of less than 10 nm.

To investigate the high pressure reaction behaviour of ($In^{3+}+Nb^{5+}$) co-doped anatase TiO_2 nanocrystals, their *in situ* Raman spectra were collected under compression and decompression conditions. Tetragonal anatase TiO_2 normally has six Raman active modes ($1A_{1g}+2B_{1g}+3E_g$).[18] Only five of them are detected here when fitting the room temperature and ambient Raman spectrum (0 GPa curve of Fig. 3a). Three Raman bands around 149.5, 199.6 and 642.4 cm^{-1} are assigned to different E_g modes while the other two peaks centering at 394.3 and 516.4 cm^{-1} are ascribed to the B_{1g} and A_{1g}/B_{1g} active modes. The Raman signal at 199.6 cm^{-1} is very weak and two different modes (A_{1g} or B_{1g}) at 516.4 cm^{-1} cannot be

distinguished unambiguously. These phenomena are common for nanoscale TiO_2 and are caused by their strong size-effects.[19]

When the achieved co-doped anatase TiO_2 nanocrystals are gradually pressurized to 47.2 GPa in a diamond anvil cell, the shift of Raman peaks and the detailed process for forming a baddeleyite-like phase are observed. Below 19.1 GPa, the four prominent Raman peaks of co-doped TiO_2 all shift to higher wavenumbers with increasing pressures. Above 19.1 GPa, a typical A_g mode of baddeleyite-like TiO_2 begins to appear at 480.2 cm^{-1} (it is labelled by a "*" symbol). This onset pressure for phase transition is much lower than that of un-doped TiO_2 with similar crystal sizes (~24 GPa, Fig. 1), but is slightly higher than that of Nb^{5+} single-doped anatase nanoparticles (~18 GPa).[20] Further increasing the external pressures, the A_g peak intensity at 480.2 cm^{-1} continuously increases and the other Raman peaks of baddeleyite-like TiO_2 become more prominent (see the Raman spectra collected at *e.g.* 21.9 and 26.0 GPa). It suggests a gradual phase transition from anatase to a baddeleyite-like structure with these two phases co-existing in the transitional region. At ~27.9 GPa, the baddeleyite-like phase completely forms and keeps stable up to the maximum pressure (47.2 GPa, Supporting Information, Figure S1). Comparing with the amorphization of un-doped anatese TiO_2 nanocrystals with a similar size distribution (Fig. 1), the phase transition behaviour of co-doped anatese TiO_2 is significantly changed due to the introduction of In^{3+} and Nb^{5+} ions.

The formed baddeleyite-like structure can only exist under HP conditions. It gradually changes to an α-PbO_2-like phase when the pressure is reduced to 32.7 GPa (*i.e.* the Raman peak of an α-PbO_2-like phase appears at ~446.8 cm^{-1}, Fig. 3b). The phase transition from a baddeleyite-like to an α-PbO_2-like structure completes at ~2.3 GPa and then the α-PbO_2-like structure remains stable even when the pressure is completely released. The co-doped α-PbO_2-like TiO_2 synthesized thereof shows $3A_g$ (175.3, 426.1 and 531.9 cm^{-1}), $3B_{1g}$ (280.6, 317.0 and 567.3 cm^{-1}), $1B_{2g}$ (346.2 cm^{-1}) and $1B_{3g}$ (156.0 cm^{-1}) Raman active modes.

For one compression and decompression cycle, $(In^{3+}+Nb^{5+})$ co-doped anatase TiO_2 nanocrystals experience the phase transition in the sequence of (1) anatase → baddeleyite-like phase (compression) → α-PbO_2-like structure (decompression, Fig. 3c). This structural transition scenario differs from the pressure-induced amorphization of un-doped TiO_2 nanoparticles with the similar crystallite sizes (<11 nm), but is more closely analogous to that of large-sized ones (11-40 nm, Fig. 1). Trans-regime structural transition is thus activated by co-doping In^{3+} and Nb^{5+} ions.

From a structural perspective, anatase and α-PbO_2-like TiO_2 are both composed of TiO_6 octahedra. The octahedral arrangements, however, are quite different between them (Fig. 3c). TiO_6 octahedra form zigzag chains along a and b directions and each octahedron shares four edges in anatase TiO_2 while they form the planar chains sharing edges in a zigzag arrangement along the c direction in an α-PbO_2-like crystal structure.[9d] Meanwhile, the baddeleyite-like phase is constructed by TiO_7 decahedra and the coordination number of Ti^{4+} cations also changes from six to seven. Hence, the structural transition of $(In^{3+}+Nb^{5+})$ co-doped anatase TiO_2 nanocrystals is complicated under HP conditions and accompanied by the breaking and reassembling of M-O chemical bonds (M represents In, Nb and Ti ions and O is oxygen.).

In order to quantatively describe the shift of Raman peaks, pressure (p) dependent Raman frequency (v) is plotted and fitted for different active modes of co-doped TiO_2 nanocrystals (Fig. 4a, 4d and 4e). The pressure coefficient (dv/dp) is about 2.20 $cm^{-1} \cdot GPa^{-1}$ for the $E_{g(1)}$ Raman mode of co-doped anatase TiO_2. It is about 12% lower than that of un-doped (2.58±0.22 $cm^{-1} \cdot GPa^{-1}$)[8d] and about 22% smaller than that of 10 at.% Nb^{5+} single-doped TiO_2 (2.81 $cm^{-1} \cdot GPa^{-1}$),[20] meaning that M-O chemical bonds of co-doped nanocrystals are more incompressible than the latter two samples. The dv/dp values of other Raman modes are also lower and presents the similar trends as that of $E_{g(1)}$ mode. Table 1 summarizes the pressure coefficients of $(In^{3+}+Nb^{5+})$ co-doped/Nb^{5+} single-doped/un-doped anatase, baddeleyite-like and α-PbO_2-like TiO_2 nanocrystals. It is obvious that Nb^{5+} ions single-doping results in larger dv/dp values and actually softens anatase TiO_2 nanoparticles.[20] However, In^{3+} and Nb^{5+} co-doping leads to an opposite variation and should harden their co-doped nanocrystals (*i.e.* enhancing their stiffness).[8b,8e,8h] In addition,

we also find a small dip in the enlarged pressure-Raman frequency curve of below 0.8 GPa (Fig. 4b) due to the pressure difference between interior and exterior of co-doped TiO_2 nanoparticles.[8b,8d] This pressure difference further results in a steep decrement and then a continuous increment of Raman line widths on both sides of ~5 GPa (Fig. 4c).

The stiffening of co-doped TiO_2 nanocrystals should be physically attributed to the synergic effects of In^{3+} and Nb^{5+} co-dopants. The Pauling ionic radii of In^{3+} ions are 94 pm in the six-coordinated octahedra and are much larger than that of Ti^{4+} (74.5 pm) or Nb^{5+} (78 pm) ions. Bond-valence-sum (BVS) calculations[21] show that In^{3+} ions (5 at.%) are strongly overbonded in anatase TiO_2 with the global instability index (GII) of 1.2402 v.u. while Nb^{5+} ions (5 at.%) are slightly overbonded with GII=0.3540 v.u. In-O chemical bonds become more incompressible than Ti-O or Nb-O bonds due to the large-size of overbonded In^{3+} ions and thus leads to the enhanced stiffness of co-doped TiO_2. However, the mono-doping level of In^{3+} ions in TiO_2 is very low and usually less than 1 at.%, which is impossible to achieve 5 at.% without phase segregation.[22] Nb^{5+} ions co-doping thus prompts the dissolution of In^{3+} ions and their associated synergistic effects enhance the stiffness of anatase nanocrystals. Based on (In^{3+}+Nb^{5+}) co-doped bulk crystals, the density functional theory (DFT) calculations were performed (Supporting Information, S3). The results show that co-doped bulk crystals become soft and are contrary to that of nanocrystals since 3D confinement of finite-sized nanoparticles cannot be considered for the DFT calculations.

The synergistic effects of In^{3+} and Nb^{5+} ions also determine the trans-regime structural transition of co-doped nanocrystals under HP conditions. Doping introduces different defect states into host materials and these intentionally introduced defects can act as heterogeneous nucleation centres of crystal-crystal transition.[23] Classical nucleation theory points out that the energy barrier (ΔG^*) of heterogeneous nucleation is always lower than that of homogeneous nucleation. It is thus energically favourable to activate the structural transition of co-doped TiO_2 nanoparticles using a smaller pressure than that of un-doped TiO_2. Experimentally, the critical pressure of phase

transition from anatase to a baddeleyite-like structure is ~19.1 GPa, which is much lower than that of un-doped samples (~24 GPa). During decompression, the similar results can also be obtained. Therefore, defect-induced heterogeneous nucleation mechanism is responsible for the observed trans-regime structural transition of co-doped nanocrystals.

Figure 5 shows a schematic of defect-induced heterogeneous nucleation mechanism. Crystal fields and chemical bonds around In^{3+} and Nb^{5+} co-doped sites are different from that of titanium and result in a non-uniform pressure distribution within co-doped TiO_2 nanoparticles under HP conditions. Locally, the crystal structure surrounding doped sites firstly distorts because the defect positions have higher energy. In-O or Nb-O chemical bonds then break down and reassemble into the basic MO_7 units of a baddelyite-like structure. During this process, the introduced defects through co-doping In^{3+} and Nb^{5+} ions serve as the nucleation centres of new polymorphs. Once the crystal nuclei are shaped, they consume other smaller ones and gradually grow into nanoparticles following the Ostwald ripening process until all co-doped anatase TiO_2 changes to a baddelyite-like phase. This crystal growth process is supported by the appearance of NbO nanoclusters during the phase transition of Nb^{5+} single-doped TiO_2 nanoparticles from anatase to rutile[23a] and it is also supported by the study on the preparation of silicon nanoparticles.[24] A similar scenario also happens in the phase transition from a baddeleyite-like to an α-PbO_2-like structure. However, it should be pointed out that the driving force for phase transition at the compression stage is quite different from that of decompression process. The former comes from the external pressure while the latter is from the interiors of nanoparticles.

CONCLUSION

High pressure reaction behaviours of (In^{3+}+Nb^{5+}) co-doped anatase TiO_2 nanocrystals (<10 nm) were investigated by an *in situ* Raman spectrometer. In^{3+} and Nb^{5+} ions co-doping not only induces trans-regime structural transition of anatase TiO_2 nanocrystals but also enhances their stiffness or incompressibility due

to the synergistic effects of co-dopants. The crystallographic evolution of co-doped TiO_2 is demonstrated to follow the sequence of anatase to a baddeleyite-like phase (under compression) and then to an α-PbO_2-like structure (under decompression). This abnormal trans-tregime structural transition is determined by the defect-induced heterogeneous nucleation mechanism. The combination of high pressure and co-doping strategy is thus critical for the synthesis of other co-doped metastable polymorphic nanomaterials and it is also significant to optimize the physicochemical properties of traditional materials.

ASSOCIATED CONTENT

Supporting Information

The Supporting Information is available free of charge for Crystal Growth & Design.

AUTHOR INFORMATION

Corresponding Author

*E-mail: yun.liu@anu.edu.au

Author Contributions

Q. S., Y. L., L. Q. H., J. E. B. and T. J. F. make the main contribution to the preparation of this manuscript. Y. L. initiated this research, planned and coordinated all experimental and theoretical work. Q. S. synthesized the nanopowders. Q. S. and L. Q. H. designed high pressure reaction experiments with the supervision of J. E. B.. T. J. F. performed the theoretical work collaborated with Y. L.. Q. S., T. L., D. Y. conducted HRTEM, SEM/EDS, XPS analysis with the collaboration of C. Z. and Z. F. All authors were involved in the data analysis and discussion as well as the manuscript preparation.

Notes

The authors declare no competing financial interest.

References

[1] McMillan, P. F. *Chem. Soc. Rev.* 2006, *35,* 855-857.

[2] McMillan, P. F. *Nat. Mater.* 2002, *1,* 19-25.

[3] Sato, H.; Endo, S.; Sugiyama, M.; Kikegawa, T.; Shimomura, O.; Kusaba, K. *Science* 1991, *251,* 786-788.

[4] Jr. G. C.; Parrino, F.; Palmisano, G.; Scandura, G.; Citro, I.; Calogero, G.; Bartolotta, A.; Marco, G. D. *Photochem. Photobiol. Sci.* 2015, *14,* 1685-1693.

[5] Kuo, M. -Y.; Chen, C. -L.; Hua, C. -Y.; Yang, H. -C.; Shen, P. *J. Phys. Chem. B* 2005, *109,* 8693-8700.

[6] (a) Kimber, S. A. J.; Kreyssig, A.; Zhang, Y. -Z.; Jeschke, H. O.; Valentí, R.; Yokaichiya, F.; Colombier, E.; Yan, J.; Hansen, T. C.; Chatterji, T.; McQueeney, R. J.; Canfield, P. C.; Goldman, A. I.; Argyriou, D. N. *Nat. Mater.* 2009, *8,* 471-475. (b) Torikachvili, M. S.; Bud'ko, S. L.; Ni, N.; Canfield, P. C. *Phys. Rev. Lett.* 2008, *101,* 057006.

[7] San-Miguel, A. *Chem. Soc. Rev.* 2006, *35,* 876-889.

[8] (a) Cai, Y.; Zhang, C.; Feng, Y. P. *Phys. Rev. B* 2011, *84,* 094107. (b) Swamy, V.; Kuznetsov, A.; Dubrovinsky, L. S.; Caruso, R. A.; Shchukin, D. G.; Muddle, B. C. *Phys. Rev. B* 2005, *71,* 184302. (c) Swamy, V.; Dubrovinsky, L. S.; Dubrovinskaia, N. A.; Langenhorst, F.; Simionovici, A. S.; Drakopoulos, M.; Dmitriev, V.; Weber, H. -P. *Solid State Commun.* 2005, *134,* 541-546. (d) Hearne, G. R.; Zhao, J.; Dawe, A. M.; Pischedda, V.; Maaza, M.; Nieuwoudt, M. K.; Kibasomba, P.; Nemraoui, O.; Comins, J. D.; Witcomb, M. J. *Phys. Rev. B* 2004, *70,* 134102. (e) Swamy, V.; Dubrovinsky, L. S.; Dubrovinskaia, N. A.; Simionovici, A. S.; Drakopoulos, M.; Dmitriev, V.; Weber, H. -P. *Solid State Commun.* 2003, *125,* 111-115. (f) Haines, J.; Léger, J. M. *Physica B* 1993, *192,* 233-237. (g) Sekiya, T.; Ohta, S.; Kamei, S.; Hanakawa, M.; Kurita, S. *J. Phys. Chem. Solids* 2001, *62,* 717-721. (h) Arlt, T.; Bermejo, M.; Blanco, M. A.; Gerward, L.; Jiang, J. Z.; Olsen, J. S.; Recio, J. M. *Phys. Rev. B* 2000, *61,* 14414-14419.

[9] (a) Zhu, T.; Gao, S. -P. *J. Phys. Chem. C* 2014, *118,* 11385-11396. (b) Fu, Z.; Liang, Y.; Wang, S.; Zhong, Z. *Phys. Status Solidi B* 2013, *250,* 2206-2214. (c) Dubrovinskaia, N. A.; Dubrovinsky, L. S.; Ahuja, R.; Prokopenko, V. B.; Dmitriev, V.; Weber, H. -P.; Osorio-Guillen, J. M.; Johansson, B. *Phys. Rev. Lett.* 2001, *87,* 275501. (d) Muscat, J.; Swamy, V.; Harrison, N. M. *Phys. Rev. B* 2002, *65,* 224112.

[10] (a) Pischedda, V.; Hearne, G. R.; Dawe, A. M.; Lowther, J. E. *Phys. Rev. Lett.* 2006, *96,* 035509. (b) Swamy, V.; Kuznetsov, A.; Dubrovinsky, L. S.; McMillan, P. F.; Prakapenka, V. B.; Shen, G.; Muddle, B. C. *Phys. Rev. Lett.* 2006, *96,* 135702. (c) Wang, Z.; Saxena, S. K. *Solid State Commun.* 2001, *118,* 75-78. (d) Wang, Z.; Saxena, S. K.; Pischedda, V.; Liermann, H. P.; Zha, C. S. *J. Phys.: Condens. Matter.* 2001, *13,* 8317-8323.

[11] Yan, X.; Gu, Y.; Zhang, X.; Huang, Y.; Qi, J.; Zhang, Y.; Fujita, T.; Chen, M. *J. Phys. Chem. C* 2009, *113,* 1164-1167.

[12] Cong, R.; Zhu, H.; Wu, X.; Ma, C.; Yin, G.; Xie, X.; Cui, Q. *J. Phys. Chem. C* 2013, *117,* 4304-4308.

[13] Yin, G.; Yin, H.; Wang, X.; Sun, M.; Zhong, L.; Cong, R.; Zhu, H.; Gao, W.; Cui, Q. *J. Alloys Compd.* 2014, *611,* 24-29.

[14] Hu, W.; Liu, Y.; Withers, R. L.; Frankcombe, T. J.; Norén, L.; Snashall, A.; Kitchin, M.; Smith, P.; Gong, B.; Chen, H.; Brink, F.; Schiemer, J.; Wong-Leung, J. *Nat. Mater.* 2013, *12,* 821-826.

[15] Liu, Y.; Fu, Z.; Sun, Q.; Withers, R. L.; Norén, L.; Zhou, C. *C. N. Patent* 201610288912, May 3, 2016.

[16] Dewaele, A.; Torrent, M.; Loubeyre, P.; Mezouar, M. *Phys. Rev. B* 2008, *78,* 104102.

[17] Sun, Q.; Zeng Y.; Jiang, D. *CrystEngComm.* 2012, *14,* 713-718.

[18] (a) Frank, O.; Zukalova, M.; Laskova, B.; Kürti, J.; Koltai, J.; Kavan, L. *Phys. Chem. Chem. Phys.* 2012, *14,* 14567-14572. (b) Ohsaka, T.; Izumi, F.; Fujiki, Y. *J. Raman spectroscopy* 1978, *7,* 321-324.

[19] (a) Tian, F.; Zhang, Y.; Zhang, J.; Pan C. *J. Phys. Chem. C* 2012, *116,* 7515-7519. (b) Sahoo, S.; Arora, A. K.; Sridharan, V. *J. Phys. Chem. C* 2009, *113,* 16927-16933.

[20] Lü, X.; Yang, W.; Quan, Z.; Lin, T.; Bai, L.; Wang, L.; Huang, F.; Zhao, Y. *J. Am. Chem. Soc.* 2014, *136,* 419-426.

[21] (a) Brown, I. D. *Acta Cryst. B* 1992, *48,* 553-572. (b) Brown, I. D. *Acta Cryst. B* 1997, *53,* 381-393. (c) For the detailed Bond valence sum calculation, please refer to the below website: http://www.softbv.

net/indexconv.html.

[22] Atanacio, A. J.; Bak, T.; Nowotny, J. *ACS Appl. Mater. Interfaces* 2012, *4,* 6626-6634.

[23] (a) Arbiol, J.; Cerdà, J.; Dezanneau, G.; Cirera, A.; Peiró, F.; Cornet, A.; Morante, J. R. *J. Appl. Phys.* 2002, *92,* 853-861. (b) Beck, H. P.; Kaliba, C. *Mat. Res. Bull.* 1991, *26,* 145-152. (c) Hanaor, D. A. H.; Sorrell, C. C. *J Mater. Sci.* 2011, **46**, 855-874.

[24] Kang, M. -K.; Kim, S. J.; Kim, H. J. *Nanoscale* 2013, *5,* 3266-3271.
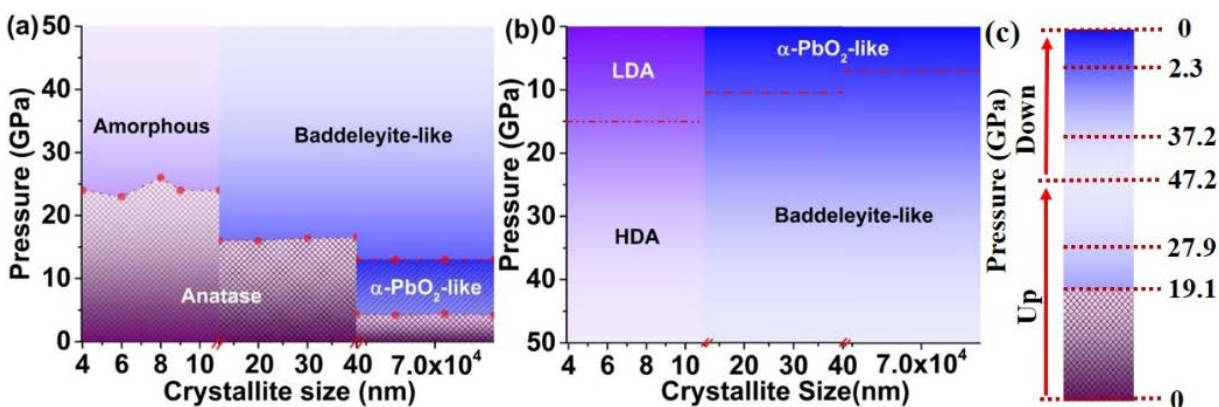
Figure Captions

Figure 1. Size-dependent compression (a) and decompression (b) phase diagrams of un-doped anatase TiO$_2$.[8-10] Three size regimes can be categorized. The dot lines label the boundary of onset structural transition. H (L) DA means a high (low)-density amorphous state. (c) shows the structural transition of (5at.% In^{3+}+5at.% Nb^{5+}) co-doped anatase TiO$_2$ nanocrystals (<10 nm) under pressurization (pressure up) and depressurization (pressure down) conditions.
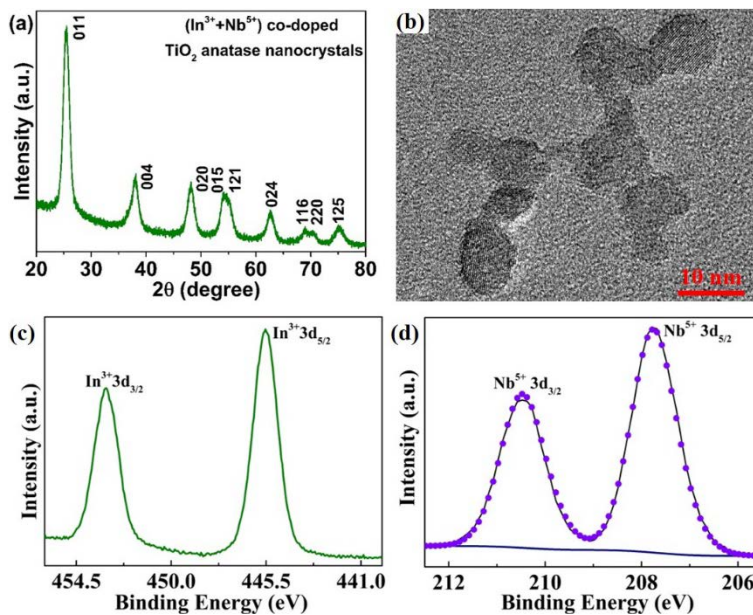

Figure 2. The XRPD pattern (a), a HRTEM image (b) and XPS data (c and d) of (5at.%In^{3+}+5at.%Nb^{5+}) co-doped anatase TiO$_2$ nanocrystals used for high pressure reaction, indicating that they have In^{3+} and

Nb[5+] doped ions, anatase structure, quasi-spherical morphology as well as uniform size distribution of less than ~10 nm.
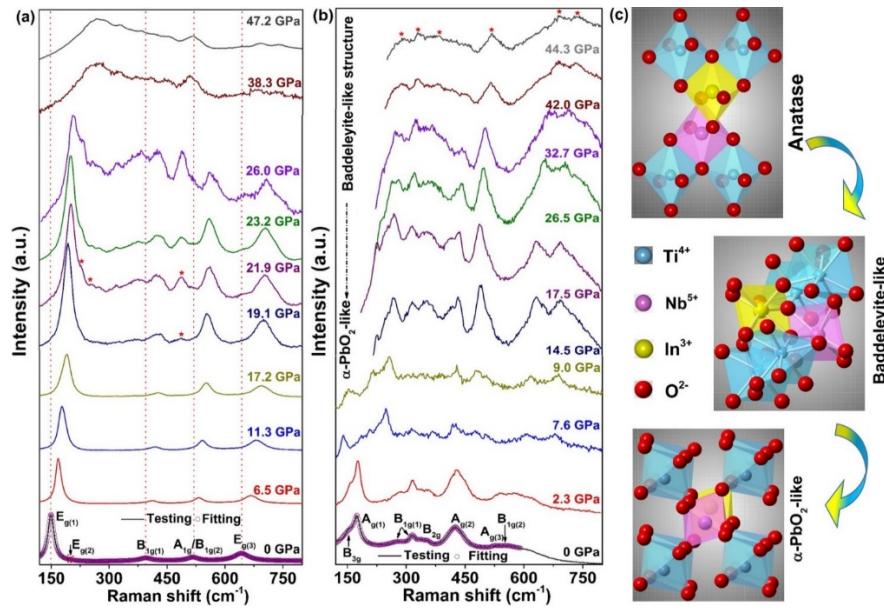

Figure 3. Raman spectra of (5at.% In[3+]+5at.% Nb[5+]) co-doped anatase TiO_2 nanocrystals collected under compression (a) and decompression (b) conditions. Their crystallographic evolution followed the sequence of anatase → baddeleyite-like phase (compression) → α-PbO_2-like structure (decompression). (c) presents the polyhedral structures of three co-doped TiO_2 polymorphs obtained in this work.
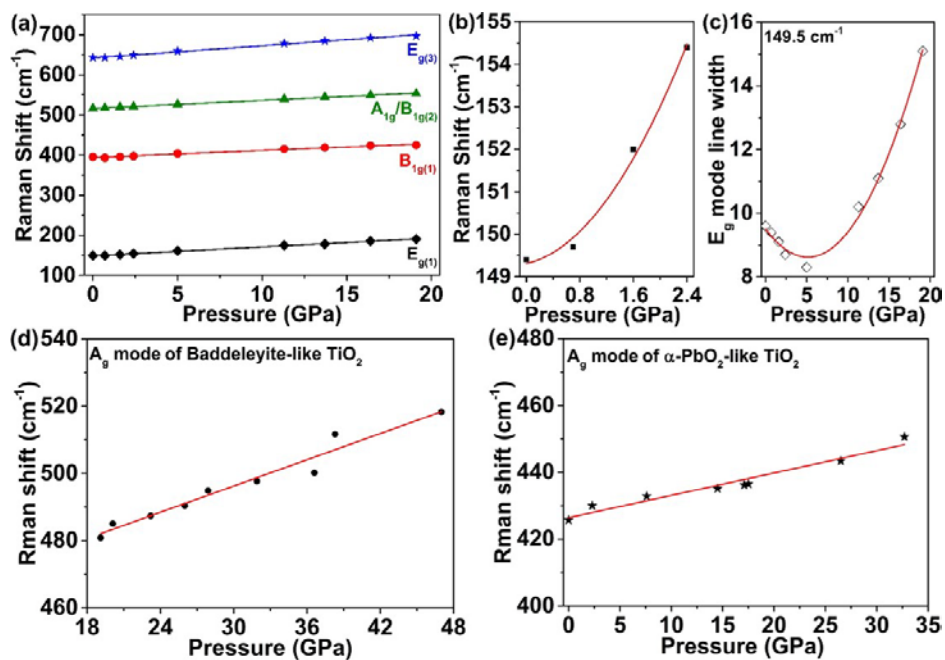

15

Figure 4. Raman frequencies of different active modes as a function of compression or decompression pressure for co-doped anatase (a), baddeleyite-like (d) and α-PbO₂-like (e) nanocrystals. (b) shows the enlarged pressure-Raman frequency curve of $E_{g(1)}$ mode of co-doped anatase TiO_2 nanocrystals at lower pressures (<2.4 GPa). (c) is the pressure-dependent Raman line width of $E_{g(1)}$ mode of co-doped anatase TiO_2 nanocrystals. The experimental data were labelled by different symbols while the linear fitting data were labelled by the solid lines.
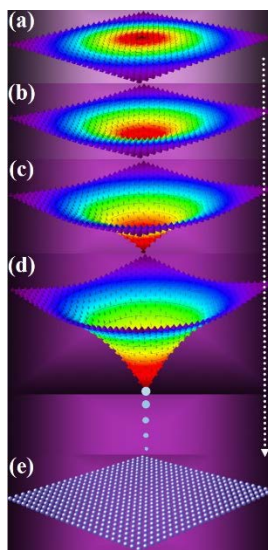

Figure 5. A schematic of the defect-induced heterogeneous nucleation mechanism. (a) Non-uniform pressure distribution among MO_6 octahedra due to their different local crystal chemistry environments (the red color represents the position of defect induced by co-doping). (b) and (c) are the distortion of local crystal structure under high pressure. (d) The formation of crystal nuclei of new phase after the breaking and reassembling of In-O, Nb-O chemical bonds. (e) The growth of new crystal nuclei into co-doped baddeleyite-like or α-PbO₂-like TiO_2 nanocrystals.

Table 1. The pressure coefficients ($d\nu/dp$) of different Raman active modes of ($In^{3+}+Nb^{5+}$) co-doped, Nb^{5+} single-doped and un-doped anatase, baddeleyite-like, α-PbO₂-like TiO_2 nanocrystals.

Crystal structures	Raman modes	dv/dp (cm^{-1}·GPa^{-1})	Samples	References
anatase	E$_g$ (149.5 cm^{-1})	2.20 ($\pm$0.05)	5at.%In^{3+}+5at.%Nb^{5+}	This work
		2.58 ($\pm$0.22)	un-doped	8d
		2.81	(10at.% Nb^{5+}) single-doped	Ref. 20
	B$_{1g}$ (394.3 cm^{-1})	1.76 ($\pm$0.08)	5at.%In^{3+}+5at.%Nb^{5+}	This work
		2.7	un-doped	Ref. 10c
		~2.8	(10at.% Nb^{5+}) single-doped	Ref. 20
	A$_{1g}$/B$_{1g}$ (516.4cm^{-1})	1.98 ($\pm$0.03)	5at.%In^{3+}+5at.%Nb^{5+}	This work
		2.7	un-doped	Ref. 10c
		~2.6	(10at.% Nb^{5+}) single-doped	Ref. 20
	E$_g$ (642.4 cm^{-1})	3.03 ($\pm$0.09)	5at.%In^{3+}+5at.%Nb^{5+}	This work
		3.1	un-doped	Ref. 10c
		~4.2	(10at.% Nb^{5+}) single-doped	Ref. 20
baddeleyite	A$_g$ (480.2 cm^{-1})	1.30 ($\pm$0.10)	5at.%In^{3+}+5at.%Nb^{5+}	This work
		1.65 ($\pm$0.21)	un-doped	Ref. 8d
α-PbO$_2$	A$_g$ (426.1 cm^{-1})	0.67 ($\pm$0.06)	5at.%In^{3+}+5at.%Nb^{5+}	This work
		~3.1	(5at.% Nb^{5+}) single-doped	Ref. 20